ACS OMEGA

http://pubs.acs.org/journal/acsodf

Article

Formation and Structure of Nanotubes in Imidazolium-Based Ionic Liquid Aqueous Solution

Guohui Zhou* and Kun Jiang

Cite This: *ACS Omega* 2022, 7, 45598−45608

Read Online

ACCESS | Metrics & More | Article Recommendations | Supporting Information

ABSTRACT: Self-assembled structures have attracted much attention for their potential applications in biological and electrochemical studies. Understanding the aggregation mechanism is necessary for utilizing the structures and improving the properties. In this study, the tubular cluster aggregations formed by the 1-dodecyl-3-methylimidazolium salicylate ([C_{12}mim][Sal]) have been studied by molecular dynamics simulations. The rod-like and funnel-shaped structures were observed during the simulations, and finally, the nanotube structure enclosed by a bilayer membrane was formed. For the first time, the point cloud fitting method was used to obtain the axis equation of the tubular cluster. Based on the equation, the structure of tubular clusters was analyzed in detail. The imidazolium ring and anions were distributed at the ionic liquid−water interface, while the dodecyl groups were buried in the nanotube membrane away from the water. Electrostatic interactions between cations and anions played a dominant role in stabilizing the structure of the nanotube. The tubular cluster size, membrane thickness, and permeability of water molecules through the membrane of the cluster were also calculated. Furthermore, the orientation analysis revealed that multitudinous aggregation structures could be formed by the long alkyl chain in aqueous solution, which might be beneficial for the strengthening and separating processes.

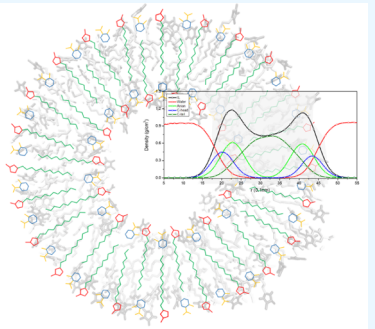

Structure of tubular cluster for [C_{12}mim][Sal]

1. INTRODUCTION

Nowadays, the development of self-assembled structures has attracted much attention for their potential applications in electrochemistry,[1−6] separation,[7−15] molecular catalysis, and drug delivery.[16−24] Building blocks commonly have amphiphilic properties. By conducting the polymer and surfactant, aggregation structures such as globular clusters, bilayers, nanotubes, and vesicles were formed and investigated.[25,26]

In recent decades, numerous studies have shown that long alkyl chain ionic liquids (ILs) can form self-aggregation structures, such as micelle and vesicular structures in aqueous solution.[27−31] Yu et al.[32,33] used surface active ILs to form the lyotropic liquid crystals and lamellar gels by adjusting the concentration and type of solvent. Lépori et al.[34] studied the characteristics of the vesicles formed by 1-butyl-3-methylimidazolium 1,4-bis(2-ethylhexoxy)-1,4-dioxobutane-2-sulfonate ([Bmim][AOT]) and 1-hexyl-3-methylimidazolium 1,4-bis(2-ethylhexoxy)-1,4-dioxobutane-2-sulfonate ([Hmim][AOT]) and found that the hydrophobic interactions played a major role in forming surfactant−DNA complexes. Apart from properties of aggregation behavior, related applications were also expanded and carried out in many studies. Li et al.[35] investigated reversible emulsification and demulsification of azobenzene-based ILs by the light irradiation, which could be used for highly efficient catalytic hydrogenation and production separation. The aggregation structures formed by ILs also provide possibilities for investigations of drug delivery.[36−38]

In order to provide a microscopic insight to understand the aggregation behavior at a molecular level, theoretical studies based on quantum mechanism and molecular dynamics (MD) simulation were employed.[4,5,31,39−41] Luo et al.[42] performed MD simulations to reveal the influence of single small molecules on self-assembly behaviors of copolymers Pluronic, hydrophilicity, and hydrophobicity. Guo et al.[43] revealed that various aggregation structures such as nanotubes and vesicles can be formed by diphenylalanine-based peptide with the Coarse-Grained MD simulations, where concentrations and hydrogen bonding interactions between peptide and water played an important role in stabilizing assembly structures. Ludwig et al.[44,45] investigated the cation−cation clusters in ILs by using DFT calculations and experimental spectroscopic methods. They suggested that the clusters formed by cooperative hydrogen bonding interactions could further influence the phase behavior of ILs at a low temperature. Sharma and Bhargava studied the aggregation behavior of multiheaded surface-active ILs in water and found that the shape and size of aggregates were directly related to the

Received: October 3, 2022
Accepted: November 15, 2022
Published: November 28, 2022

https://doi.org/10.1021/acsomega.2c06381
ACS Omega 2022, 7, 45598−45608

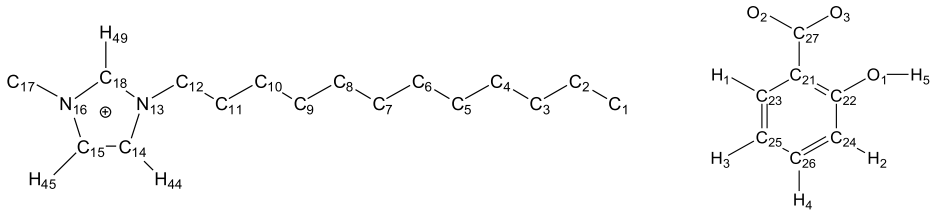

Figure 1. Structure of the cation and anion. (a) $[C_{12}mim]^+$ cation, (b) $[Sal]^-$ anion.

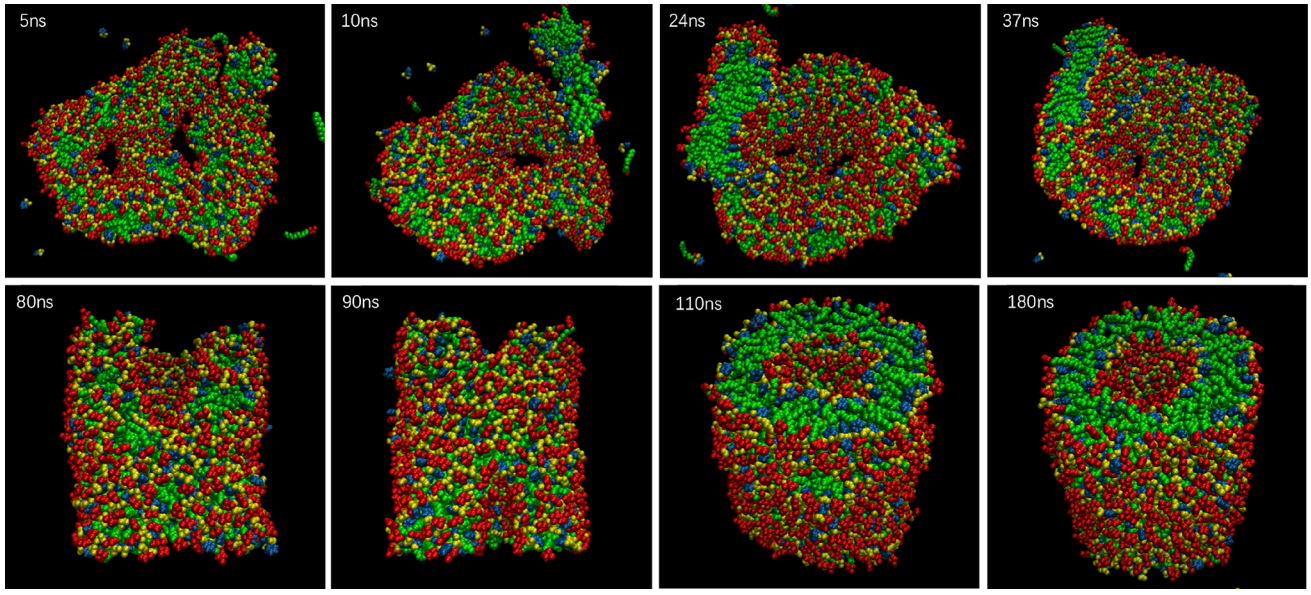

Figure 2. Aggregation process of ILs from random ILs into a tubular cluster in system 1.8. Red: imidazolium ring and methyl in the cation; green, alkyl chain in the cation; yellow: carbonyl and hydroxyl groups of anions; and dark blue: benzene ring of anions. Snapshots are shown at 5, 10, 24, 37, 80, 90, 110, and 180 ns, respectively.

number of charged head group of cations.[46] Nadimi et al. studied the aggregation behavior of two kinds of amino acid ILs in aqueous, they found that both of them can aggregate quasi spherical clusters, and hydrogen bonding was the fundamental reason for their aggregation.[47]

Furthermore, many simulations for the self-aggregation of ILs in aqueous were performed. Zhou et al.[48] found that the chain-like structure could be formed in the [Bmim][oAc]−water system at low water concentrations, which influenced the viscosity greatly. Liu et al.[49] proposed that the hydrogen bonding interaction was an important factor affecting aggregation structures of 1-dodecyl-3-methyl-imidazolium bromide ($[C_{12}mim]Br$) in vesicles and micelles. The vesicle formation process of 1-dodecyl-3-methylimidazolium salicylate ($[C_{12}mim][Sal]$) was then simulated and permeability of vesicles were evaluated as the temperature increasing.[30]

In the various aggregation structures, the tubular cluster could enhance the effect by using the interior and exterior components with the tubular wall. However, most of the above research studies are about globular clusters, micelles and vesicles, and few studies on tubular cluster have been reported.[43] In this work, the aqueous solution of $[C_{12}mim]$-[Sal] was studied by MD simulations. A stable nanotube structure was obtained, and the formation mechanism was analyzed. For the first time, the point cloud fitting method was used to obtain the equation of tube-like cluster. Based on the equation, the structure of the cluster was studied in detail, and wall thickness, distribution of cation and cation in wall surface, and the orientation were obtained. In addition, it was found that the permeability of water molecules through the membrane was almost the same in two tube clusters of different radii, both of which were lower than that in the vesicle. Besides, energy analysis indicates that the interaction between cations and anions play a dominant role in forming and stabilizing the structure.

2. SIMULATION DETAIL

MD simulations of $[C_{12}mim][Sal]$ in aqueous solution were performed based on the united-atom atomic field. Molecular structures of the cation and anion are shown in Figure 1. Topology files based on the GROMOS force field[50] are obtained by using the ATB tool.[51] The Coulombic interaction is important in ILs, so we redistribute the atomic charge by fitting the electrostatic potential surface of the cation and anion. As the SPC model water[52] has been used in the IL aqueous system,[30,31] and the results could be verified by experiments, we also chose the SPC model in this work. Besides, the OH bond in the water molecule is flexible.

Two systems sized differently are used for comparative analysis. The lengths of boxes in *XY* directions are 1.5 and 1.8 times longer than that in the *Z* direction, that is, the ratios of boxes in the *XYZ* direction are 1.5:1.5:1.0 and 1.8:1.8:1.0, which are named system 1.5 and system 1.8 in the following text. Each system contains 800 ILs and 80,000 water molecules

https://doi.org/10.1021/acsomega.2c06381
ACS Omega 2022, 7, 45598−45608

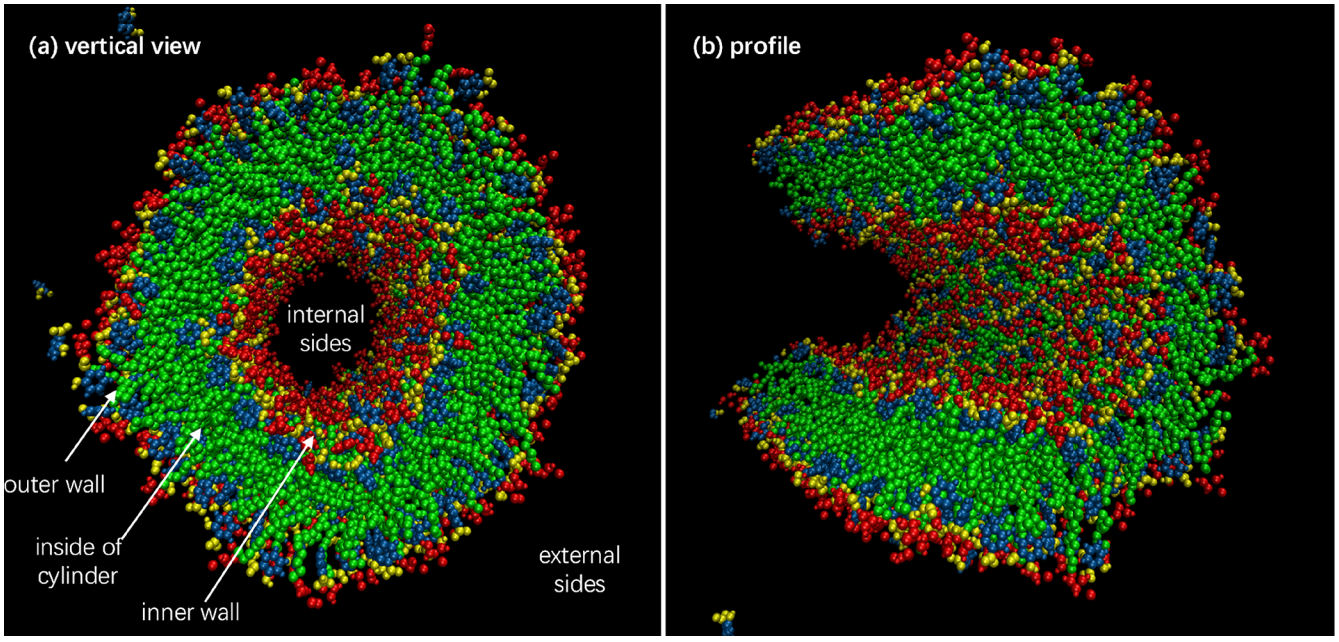

Figure 3. Screenshot of simulation up to 200 ns in system 1.8. Red: imidazolium ring and methyl in the cation, polar groups; green, alkyl chain in the cation, non-polar groups; yellow: carbonyl and hydroxyl groups of anions, polar groups; and dark blue: benzene ring of anions, nonpolar group.

(17.7 wt %). All of the simulations started with a random distribution of IL in the water, and the initial configurations were generated by the Packmol package.[53] The simulations were performed with GROMACS software package.[54,55] The two systems were, respectively, simulated at 200 ns under NPT ensemble. In order to accelerate the simulation process, the simulations were carried out at 350 K and a cutoff of 1.2 nm was set for both Lennard-Jones (LJ) and Coulombic interaction.[30] The all-bond constraints setting is used to improve the simulation speed. The standard Lorentz–Berthelot rule was used to calculate the cross interaction between different types of atoms, and the particle mesh Ewald method[56] was used to calculate the remote electrostatic interaction. Temperature was controlled with the Nosé–Hoover thermostat, coupling time was set to 0.2 ps and the pressure was maintained at 1.0 bar, and the Parrinello–Rahman constant voltage coupling time was 2.0 ps.

3. RESULTS AND DISCUSSION

3.1. Process of Cluster Formation. Figure 2 illustrates the aggregation process of tubular clusters in system 1.8. Very shortly after the simulation began, the IL rapidly aggregated into a number of small clusters, and then, they were linked to each other into several rod-shaped clusters. After that, the rod-shaped clusters connected with each other to form a sheet. At 24 ns, almost all ions assembled to a funnel, with two holes at the bottom. At 37 ns, the holes at the bottom merged into one. As the simulation proceeds, the bottom hole becomes a cylinder in the end. This process is similar to the zipper chain, half closed at 80 ns, and completely closed at 110 ns. Finally, the aggregation forms a perfect tubular cluster.

The profile of the final configuration is shown in Figure 3. Inner and outer walls of the cylinder are polar groups, which include the imidazolium ring of cation and carbonyl and hydroxyl groups on anions. In fact, the internal and external sides of the cylinder are filled with polar water molecules. From the outer wall to the inside, the benzene ring of the anion and the alkyl chain of the cation are displaced. The same arrangement is presented in Figure 3b in the axial direction.

3.2. Radial Density Distribution. Because the final configuration is a tubular cluster, the radial density distribution (RDD) is better for understanding the size and structure of the tube. Different from the spherical vesicles,[30] tubular clusters cannot be described based on the center of cluster. In order to obtain the axis equation and mean radius of the cylinder, we use the point cloud fitting method, which has been used in mapping data processing,[57] and the schematic diagram of cylindrical structure is shown in Figure 4.

In order to improve the fitting speed and accuracy of results, we have carried on special processing to the initial value

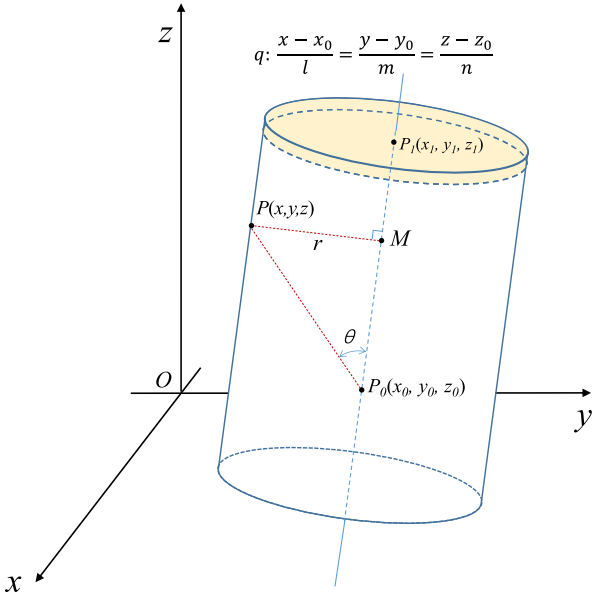

Figure 4. Schematic diagram of the cylindrical structure for point cloud fitting.

https://doi.org/10.1021/acsomega.2c06381
ACS Omega 2022, 7, 45598−45608

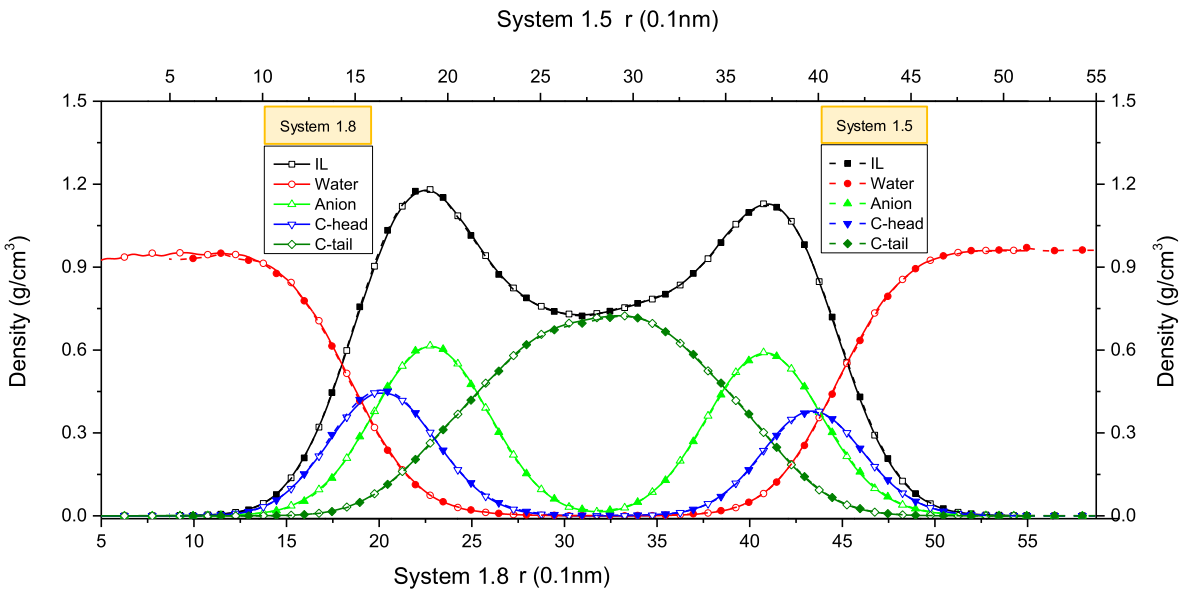

Figure 5. Radial mass density distribution of the two systems.

selection of each iteration. For the initial value selection of the configuration fitting, the mass center of all ILs (P_0) was selected to obtain the initial values of x_0, y_0, and z_0. A slice was taken at the end of tubular cluster, and the mass center of all ILs in the slice was calculated, which is denoted as P_1. The line between P_1 and P_0 is the approximate axis of the cylinder, so as to obtain the initial values of l, m, and n. Radius r can be estimated based on the structure in Figure 3. Then, the initial values of all seven parameters were obtained. In the iteration process, the deviant points representing the atoms in free ions were eliminated. Finally, a result of conformational cluster fitting was obtained by iterative convergence. To improve the iteration rate and simplify the processing, we directly used the result from the previous conformation as the initial value of the second configuration. In fact, the cluster moves very slowly and has a stable axis. According to the distance between the ions and the axis, the free ions were excluded, and then, the regression was carried out.

Figure 5 is the result of the RDD including anions, cations head (C-head), cations tail (C-tail), ILs, and water. The density distribution of ILs presents a bimodal structure. The density is high at the inner and outer wall surfaces of the cylinder, while the density is low in the middle. The high density imidazolium ring and carbonyl group are distributed on the surface of the wall, while the low density alkyl chain is distributed in the central region. The RDD of anions shows two more prominent peaks, and the anions were distributed primarily near the surface and closed to the head of cations. For cations, the central part is almost entirely alkyl chain (C-tail), and the head (C-head) is distributed on both sides. Water molecules are mainly distributed near polar groups at the surface. The inside of the cylinder is occupied by non-polar groups, and there are only very few water molecules. In Section 3.7, the diffusion behavior of water molecules through the wall will be further discussed. In order to compare the differences between the two systems, RDDs of the two systems are gathered in Figure 5. It can be seen that the density distributions of anions, cations, and ILs in two systems are almost identical.

3.3. Size of Cluster. The size of the tubular cluster was calculated based on the RDD result. The same method as the previous work[30] was adopted to define cluster boundary by density peak of cation head. According to the data in Figure 5, RDD data at the inner and outer walls were calculated, and cluster structures are listed in Table 1.

Table 1. Cluster Structures for the Two Systems

	inner wall		outer wall			
system	peak height of IL (g/cm^3)	radii (Å)[a]	peak height of IL (g/cm^3)	radii (Å)[a]	different of inner and outer peak (%)	thickness (Å)
1.8	1.180	19.90	1.131	43.40	4.3	23.50
1.5	1.180	16.25	1.127	39.75	4.7	23.50
vesicles[b]	1.175	21.20	1.091	44.20	7.7	23.00

[a]Radii of the tubular cluster are based on the location of the cation head (C-head in Figure 5) peak. [b]All vesicle data are obtained from ref 30.

For system 1.8, the maximum density of the inner wall is 1.180 g/cm^3, which is 4.3% higher than that of the outer wall. Comparing with two systems, the density of the inner wall in system 1.5 is the same with that in system 1.8, while the outer wall density is lower than that in system 1.8. This is related to the radius of curvature of the cylinder, the shorter the radius of curvature, the bigger the density difference between inner and outer walls. For the vesicles, the density of the inner wall is almost the same as that of the column cluster, but the density of the outer wall is much smaller, with a difference of 7.7% between the inner and outer walls.[30] Based on the above data, it can be found that the density of the inner wall surface is similar in different types and sizes of clusters. However, the density of the outer wall surface is quite different, and the column cluster is inversely proportional to the radius of curvature. For the similar radius, the outer wall of the vesicle has a lower density. According to the data of C-head peak, radii of inner and outer walls are 16.25 and 39.75 Å in system 1.5, respectively. In system 1.8, radii of inner and outer walls are 19.90 and 43.40 Å, which are both increased by 3.65 Å

https://doi.org/10.1021/acsomega.2c06381
ACS Omega 2022, 7, 45598−45608

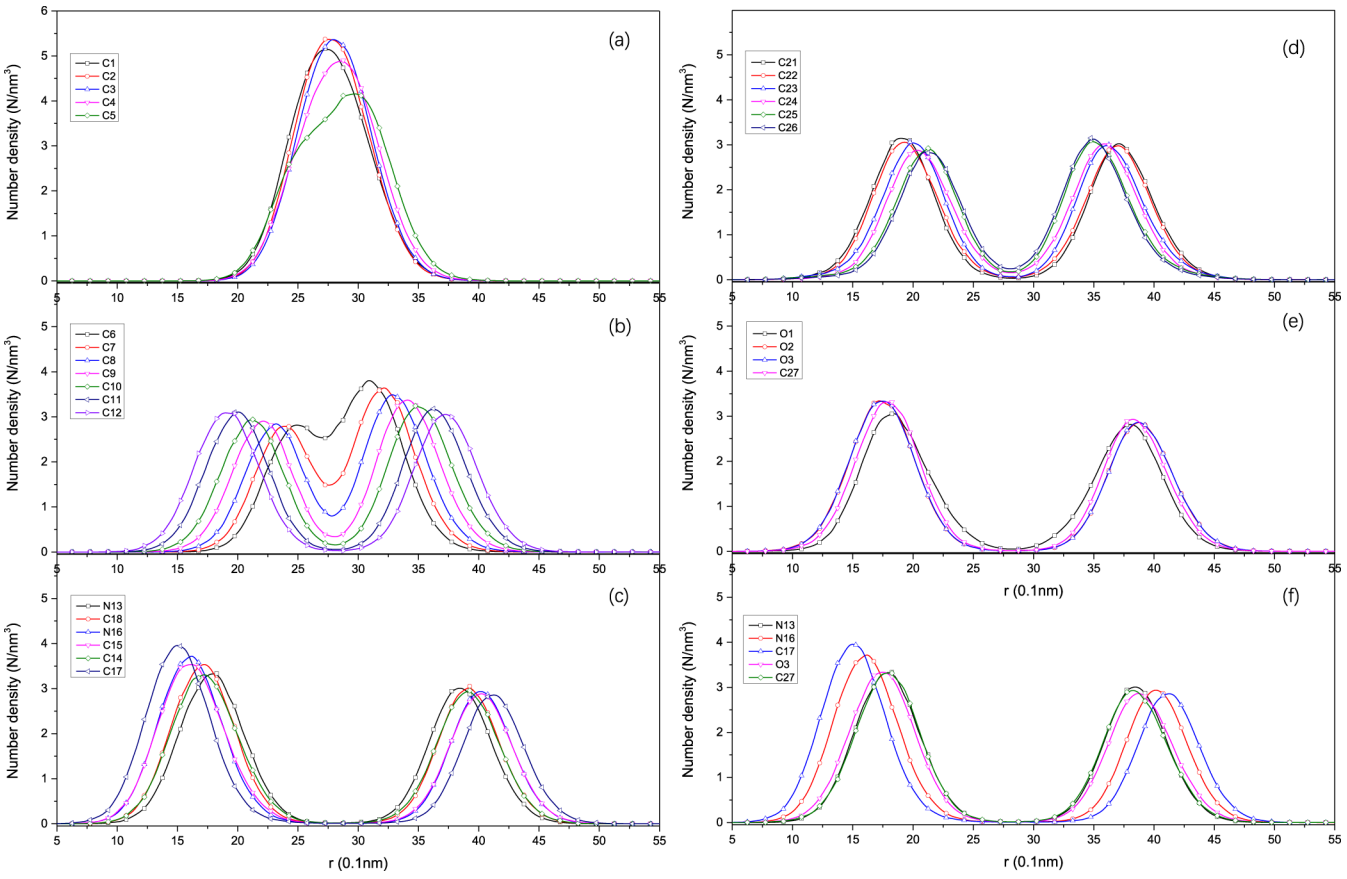

Figure 6. RND of system 1.5. (a) For five carbons at the end of the alkyl chain (C1−C5), (b) for C6 to C12 in the alkyl chain, (c) for C and N atoms on the imidazolium ring and methyl, (d) for C atoms on the benzene ring of the anion, (e) for O atoms on hydroxyl or carboxyl groups, and (f) for atoms of polar groups in the cation (N13, N16, and C17) and the anion (O3 and C27).

comparing with system 1.5. Therefore, the wall thickness of the two systems is the same and also similar to that of the vesicles (23.0 Å).[30] As the structures of the two systems are very similar, we will only focus on system 1.5 in the following parts, and the data for system 1.8 are shown in the Supporting Information.

3.4. Radius Number Density. To better understand the structure of tubular clusters, the radius number density (RND) of each atom in the cation and anion was calculated and illustrated in Figure 6. The alkyl chain contributes the main part of the non-polar region of the tubular cluster. Figure 6a shows the case of the five carbons at the end of the alkyl chain (C1−C5), all of which have only one peak, indicating that the end of the alkyl chain is intertwined. In Figure 6b, the peak began to split from C6 to C12, and the valley between the two peaks became deeper and deeper. At the same time, the peak moved toward the wall, and RND of C11 and C12 has been split completely.

The imidazolium ring and methyl are the main part of the polar region of the tubular cluster. The peaks in RND of C/N on imidazolium ring and methyl (Figure 6c) are all bimodal and have almost no overlap, indicating that they are distributed on inner or outer walls. Among these atoms, N13, which is adjacent to the long alkyl chain, is distributed in the innermost layer, while C17 on the methyl group is distributed in the outmost layer.

The carboxyl group of the anion is a polar region, whereas the benzene ring is a non-polar region. Anions are smaller than cations, especially in length. Therefore, no matter the C atom on the benzene ring (Figure 6d) or the O atom on hydroxyl or carboxyl groups (Figure 6e), all show the obvious bimodal structure. From the outside to the inside, it is the O atom on the carboxyl group, the C atom on the carboxyl group, C21 connected to the carboxyl group on the benzene ring directly, and C26 opposites to C21. The O atom on the carboxyl group appears at the same position as C and N on the imidazolium ring because they are linked by hydrogen bonds, as shown in Figure 7a.

3.5. Radial Distribution Function and Interaction Energy. To explore the microstructure, radial distribution function (RDF) was calculated to investigate the spatial distribution of cation/anion and ILs/water. Figure 7a shows the RDF of three hydrogens (H44, H45, and H49 in Figure 1a) on the imidazolium ring and carbonyl oxygen (OM is O2 and O3 in Figure 1b). It can be seen that an extremely strong interaction exists between cations and anions, making them closely connected with each other. Two anions are linked by a hydrogen bond between hydroxyl hydrogen (H5) and carbonyl oxygen (OM), as shown in Figure 7b. The RDFs of three hydrogens on the imidazolium ring and oxygen atom (OW) in water are presented in Figure 7c. Figure 7d is RDF for H (H5 in Figure 1b) on the anionic hydroxyl group and oxygen (OW) in water, as well as RDF for H (H) atoms in water and oxygen (OM) atoms in carbonyl groups. Hydrogen bond is formed between anions and water via H−OM. The interaction between cations and water is weaker comparing with anions−water. In conclusion, there is a strong interaction between the cation and anion, which is mainly reflected in the

https://doi.org/10.1021/acsomega.2c06381
ACS Omega 2022, 7, 45598−45608

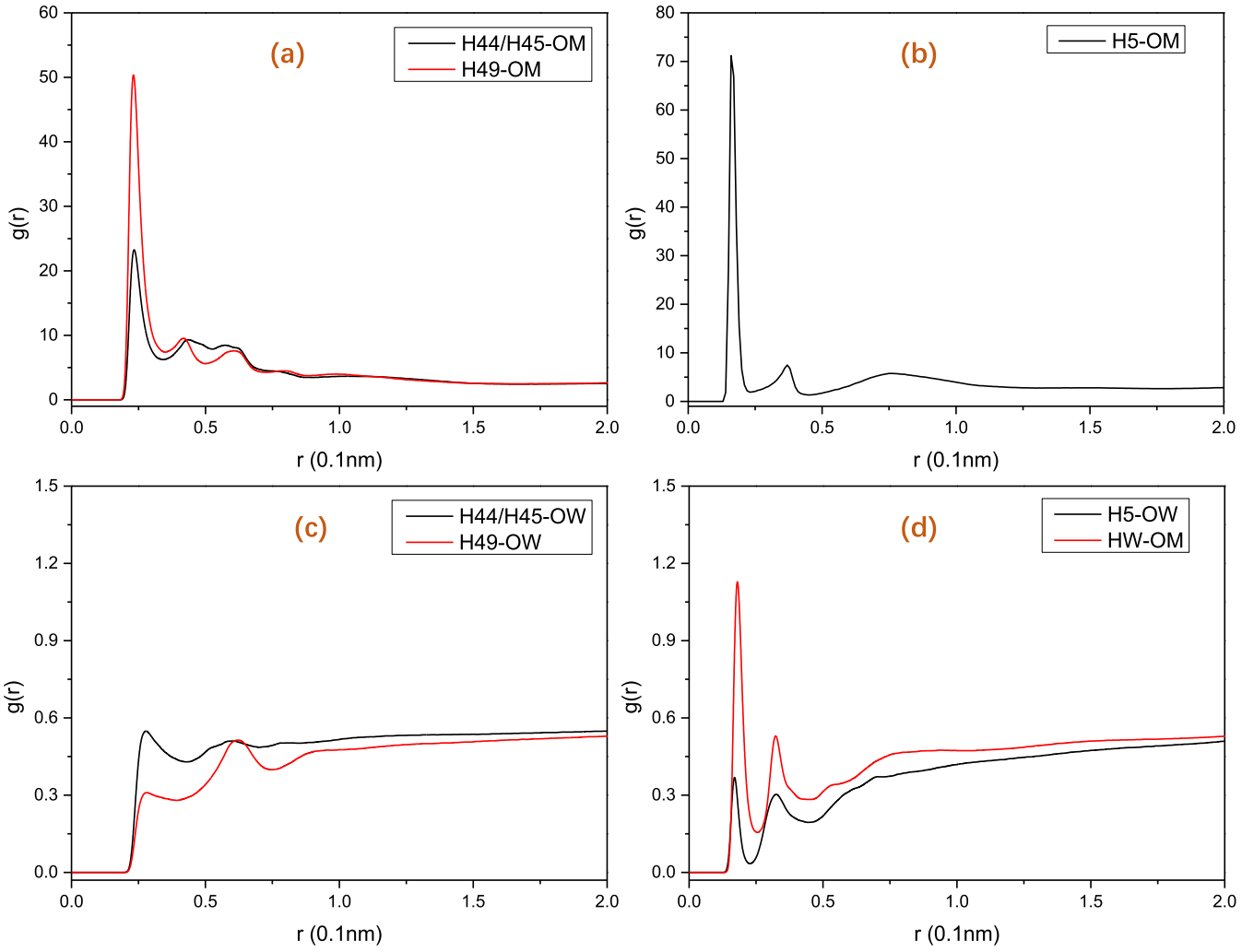

Figure 7. RDF of system 1.5. (a) RDF between three hydrogens (H44, H45, and H49) on the imidazolium ring and carbonyl oxygen (OM is O2 and O3), (b) RDF between hydrogen (H5 in Figure 1b) on the anionic hydroxyl group and oxygen (OM) in carbonyl groups. (c) RDF between three hydrogens (H44, H45, and H49) on the imidazolium ring and oxygen in water (OW), (d) RDF between hydrogen (H5 in Figure 1b) on the anion hydroxyl group and oxygen (OW) in water and the RDF between hydrogens (HW) in water and oxygen (OM) in carbonyl groups.

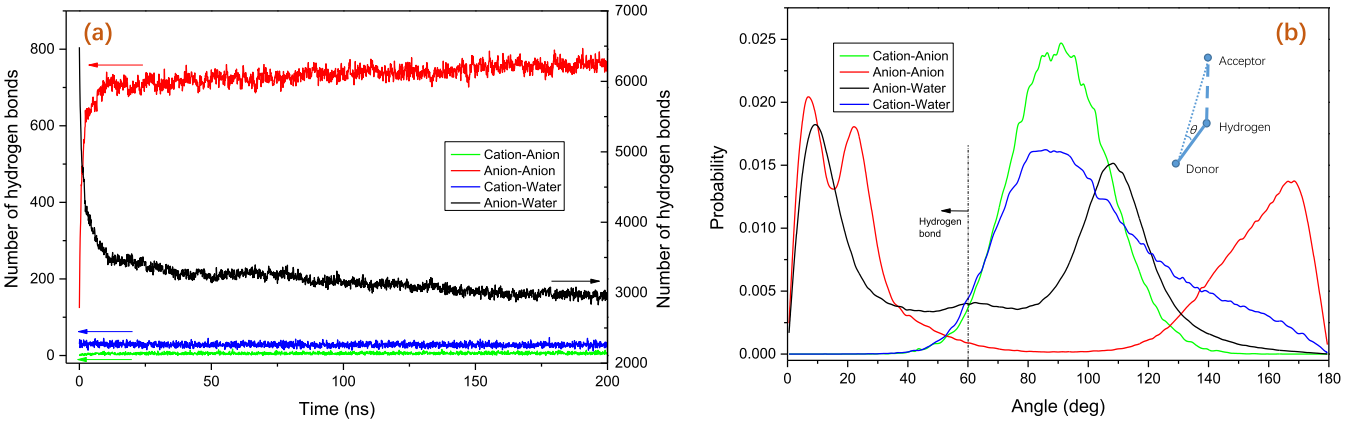

Figure 8. Hydrogen bond in system 1.5. (a) Number of hydrogen bonds over time. (b) Hydrogen bond angle distribution.

strong interaction between hydrogens on the imidazolium ring and oxygen on carbonyl groups. The interaction between oxygen on the anion carbonyl group and hydrogen in water is the main part of the interaction between IL and water.

We have calculated and analyzed the number of hydrogen bonds in system 1.5, which was used to determine the role of hydrogen bonds during the clustering of ILs. The hydrogen bond was defined as follows: the angle hydrogen−donor−acceptor is less than 60° and the distance donor−acceptor is less than 0.35 nm. The number of hydrogen bonds between the anion and water indicate a rapid decline, and the number of hydrogen bonds between anions indicates a rapid rise

https://doi.org/10.1021/acsomega.2c06381
ACS Omega 2022, 7, 45598−45608

(Figure 8a). However, the cation−anion and cation−water hydrogen bonds are not strong, as the angle is mainly distributed around 90°(Figure 8b). Therefore, the hydrogen bond between anions plays a major role in the process of aggregation, while cation-related hydrogen bonds play a minor role.

Intermolecular energy is an important factor affecting the structural stability of tubular clusters. The energy was calculated for the formation of tubular clusters (150−200 ns) and shown in Table 2. Similar to the previous algorithm,

Table 2. Intermolecular Energy for $[C_{12}mim][Sal]$ in Aqueous Solution (C, Cation; A, Anion; W, Water; H, Head of Cation; and T, Tail of Anion)

item	electrostatic ($kJ\cdot mol^{-1}$)	LJ ($kJ\cdot mol^{-1}$)	intermolecular energy ($kJ\cdot mol^{-1}$)
C−C	1006.0 ± 3.7	−48.0 ± 0.3	958.1 ± 3.5
A−A	976.0 ± 6.3	−3.8 ± 0.2	972.2 ± 6.3
C−A	−2429.4 ± 7.8	−60.0 ± 0.3	−2489.4 ± 7.9
C−W	22.7 ± 8.1	−20.0 ± 0.3	2.6 ± 8.1
A−W	−205.2 ± 14.8	10.1 ± 0.4	−195.1 ± 14.8
H−H	712.6 ± 2.8	−5.8 ± 0.1	706.7 ± 2.8
T−T	32.2 ± 0.2	−34.8 ± 0.2	−2.6 ± 0.2
H−T	261.3 ± 1.0	−7.3 ± 0.1	254.0 ± 0.9
H−A	−2041.8 ± 6.9	−27.7 ± 0.2	−2069.6 ± 7.0
T−A	−387.5 ± 1.5	−32.3 ± 0.2	−419.8 ± 1.6
H−W	9.2 ± 7.8	−16.8 ± 0.2	−7.6 ± 7.8
T−W	13.1 ± 1.9	−3.2 ± 0.1	9.8 ± 1.9

the cutoff radius of 1.6 nm was selected to improve the computational accuracy. Electrostatic attraction between the cation and anion is a central part of the total interaction, which far exceeds the repulsion between ions and plays a key role in the stability of tubular clusters. According to Figure 6f, RDD shows that methyl C17 and adjacent N16 of the imidazolium ring are more external than O3 on the anion hydroxyl group. However, the results of energy analysis show that the interaction energy between the head of the cation and water is close to zero, which is much lower than that between anion and water. The RDF results also show that water tends to bind to anions rather than imidazolium rings. Consequently, the central stable factor of tubular clusters is the C−A and A−W interaction energy.

3.6. Angle Distribution. In order to analyze the direction of the alkyl chain in the cations, we define the line between terminal carbon C1 (P_{C1}) and carbon atom C12 (P_{C12}) to represent the direction of the alkyl chain. First, the vertical point (V_{C12}) of P_{C12} on the cylindrical axis is obtained, and then, the angle of $P_{C1}-P_{C12}-V_{C12}$ is calculated. As can be seen from Figure 9a, the directions of cation alkyl chain on inner and outer walls are obviously different. Therefore, the lowest point of RND of C12 atoms is taken as the cutoff point (see Figure 6b, 28.75 Å in system 1.5), and the distribution of the alkyl chain of cations on the inner and outer walls is calculated, respectively, as shown in Figure 9b. Among them, ① is the angle distribution of outer cation alkyl chain, almost all of which are acute angles, that is, the alkyl chain is parallel to the normal direction of the wall, pointing to the inside of the cylinder; ② is the angle distribution of the inner cation alkyl chain, which is almost obtuse angle and points to the outside of the cylinder.

Similarly, the profile of the anionic angle was depicted, which indicates the direction of the benzene ring by the line between the carbon atom C27 (P_{C27}) on the carbonyl group and its opposite C26 (P_{C26}) atom. The vertical point (V_{C27}) of P_{C27} on the cylindrical axis is obtained, and the angle of $P_{C26}-P_{C27}-V_{C27}$ is calculated. In the same way, the inside and outside of the cylinder are calculated separately, and the results are shown in Figure 9c. It is clear that the benzene ring is closer to the middle of the cylinder layer, and the carbonyl tends to be distributed on the outside, which is highly consistent with the results of the cation alkyl chain.

Besides the orientation of the alkyl chain and benzene ring, the angles for imidazolium ring plane and benzene ring plane were also analyzed, as shown in Figure 10. The inner and outer angle distribution patterns of the two are similar, most of which are within the range of 30−150°, and the proportion of small angles is very low. The angle distribution of benzene rings is similar to that of imidazolium rings, and it also tends to be perpendicular to the axis of the cylinder. Such a structure is more conducive to forming $\pi-\pi$ interaction and improving the stability of the cluster.

3.7. Spatial Distribution Functions. In order to study the distribution of the imidazole ring and benzene ring, the corresponding spatial distribution functions were calculated and shown using VMD software.[58] Three carbon atoms C14, C15, and C18 were used to represent imidazole rings, and three carbon atoms C21, C24, and C25 were used to represent benzene rings. The distribution of imidazole and benzene rings around anions is shown in Figure 11a,b and that around cations is shown in Figure 11c,d. There are three main regions surrounding anions. One is the anion on the left side of Figure 11a, which is mainly connected by the H5−OM hydrogen bond. The other two are benzene and imidazole rings that are parallel to the benzene ring, and these ions get close to each other through $\pi-\pi$ interactions. From Figure 11c, we can see that there are almost no other cations around the cationic imidazole ring in the first solvation shell, and the anions are concentrated in two regions. One is the perpendicular parts to the imidazole ring, which is mainly bonded by hydrogen bonds, and the other is the parallel parts to the imidazole ring, which is mainly bonded by $\pi-\pi$ interaction. Therefore, although the $\pi-\pi$ effect is not as strong as the hydrogen bond, it also plays an important role in the stability of the structure.

Based on the above analysis, we believe that the nanotube has a layered structure. In each layer, the polar groups between anions are connected by strong hydrogen bonds. In the adjacent layers, there are $\pi-\pi$ interaction between imidazole and benzene rings and van der Waals interaction between nonpolar alkyl chains. The structural schematic diagram of the cross-section of tubular clusters is shown in Figure 12. Figure 13 is a simulated snapshot of the lateral side of the tubular cluster, and one block represents one layer. It can be seen that imidazole and benzene rings is staggered up and down, so that $\pi-\pi$ interaction is easily formed between imidazole and benzene rings, but is difficult between imidazole rings or benzene rings. Xu et al.[59] studied the morphology of $[C_{12}mim][Sal]$ in aqueous solution through experiments and DFT simulation, and concluded that $[C_{12}mim][Sal]$ aggregates in water could form tubular clusters. The structure of IL at the interface is consistent with our simulation results.

3.8. Permeability of Water Molecules. Considering the periodic boundary, water molecules are enclosed in the cluster

https://doi.org/10.1021/acsomega.2c06381
ACS Omega 2022, 7, 45598−45608

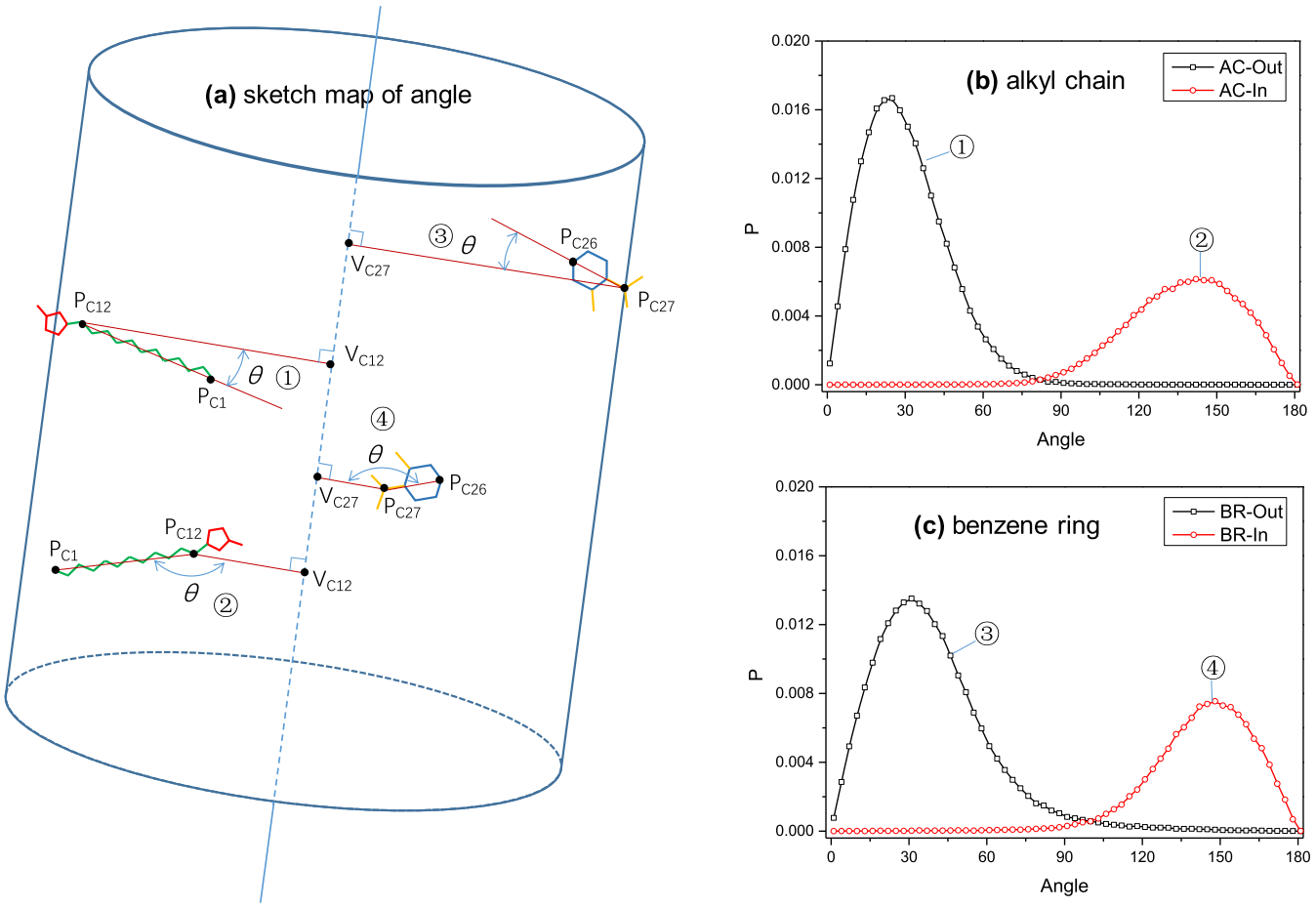

Figure 9. Angle distribution of the alkyl chain and benzene ring in system 1.5. (a) Angle diagram, (b) angle distribution of the alkyl chain, and (c) angle distribution of the benzene ring.

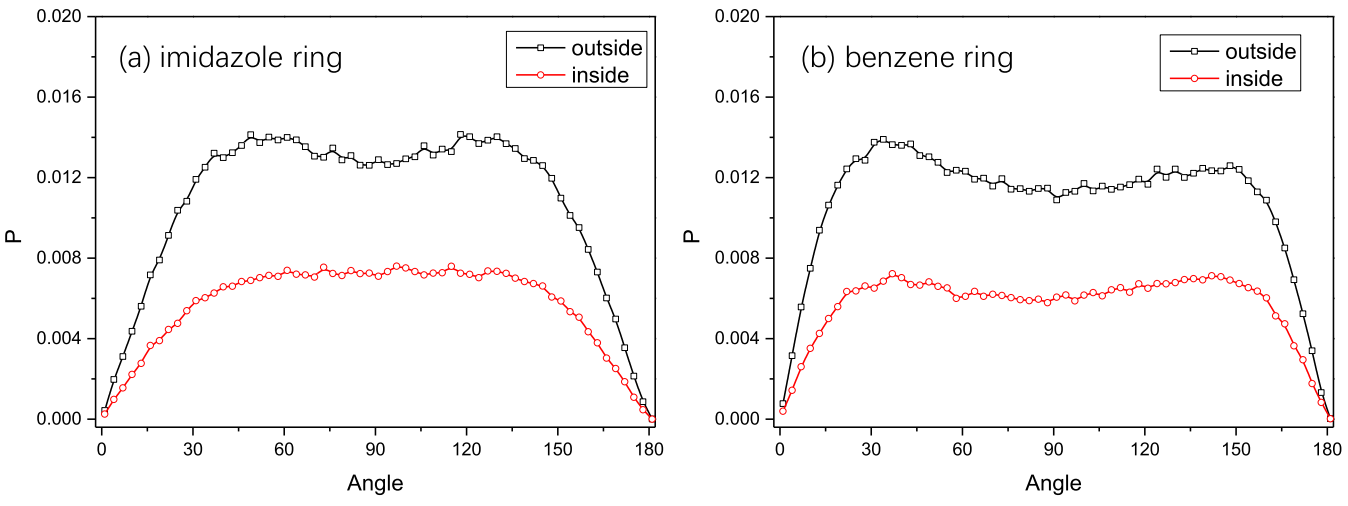

Figure 10. Imidazolium ring and benzene ring and axis angle distribution in system 1.5. (a) Angle between the imidazolium ring plane and cylindrical axis, (b) angle between the benzene ring plane and cylindrical axis.

and cannot escape from the ends of the tubular cluster. However, the wall of the cluster provides the channel for water molecules exchanging with the external molecules. At the initial time t_0, the water molecules in a tubular cluster were a set, and the boundary was radius obtained when fitting the cylinder. The number of water molecules through the wall form t_0 to t was calculated by ensemble averaging method and listed in Table 3. In system 1.5, the average number of water molecules passing through the wall is 1.09 per ns, which is slightly higher than that of system 1.8. The transfer rate of water molecules through the wall was calculated. The water transfer rate in tubular cluster is slightly lower than that in the vesicle. The results show that the shape and size of the clusters

https://doi.org/10.1021/acsomega.2c06381
ACS Omega 2022, 7, 45598−45608

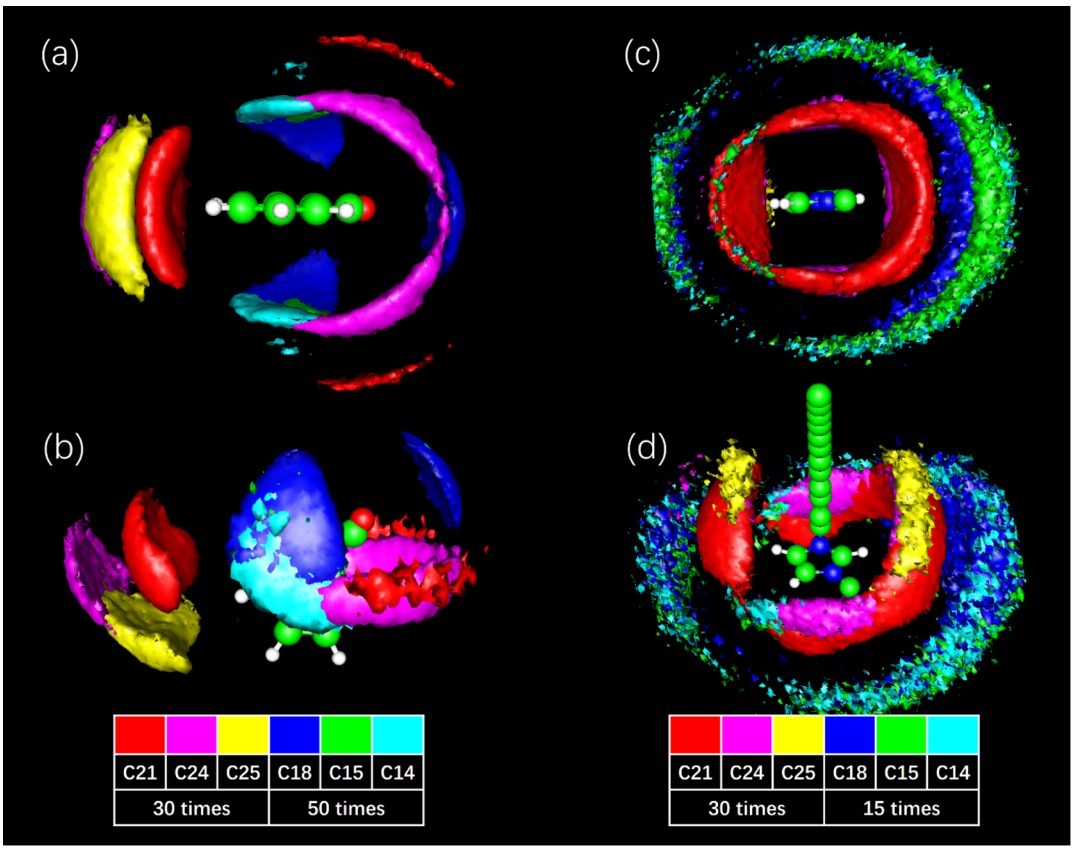

Figure 11. Spatial distribution around the cation and anion. (a,b) Distribution of benzene and imidazole rings around anions: (a) top view, (b) front view. In (a) and (b), the atom densities of C21, C24, and C25 are 30 times the average density, and the atom densities of C18, C15, and C14 are 50 times the average density. (c,d) Distribution of benzene and imidazole rings around cations: (c) top view, (d) front view. In (c) and (d), the atom densities of C21, C24, and C25 are 30 times the average density, and the atom densities of C18, C15, and C14 are 15 times the average density. Note: the legend shows the color of each atom.

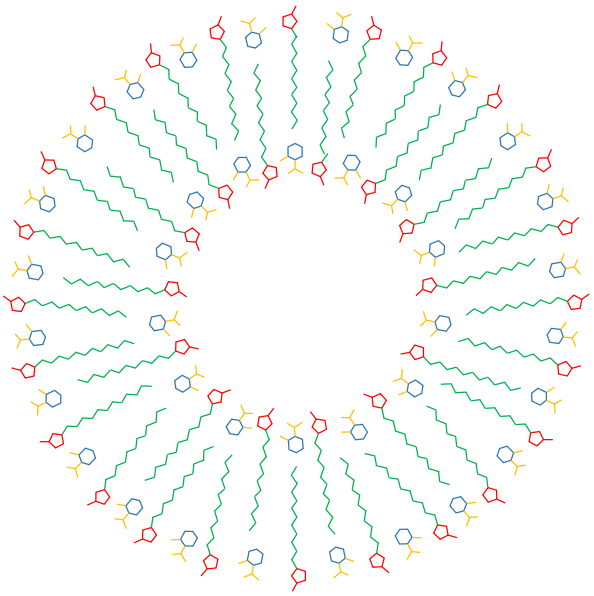

Figure 12. Structural schematic diagram of the cross-section of tubular clusters.

have an effect on the transfer rate of water molecules through the wall.

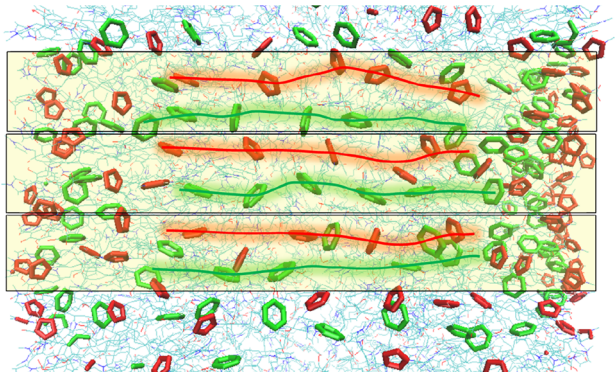

Figure 13. Profile of the simulation snapshot, green is the benzene ring, and red is the imidazole ring.

Table 3. Cluster Size and the Transform Rate of Water Molecules through the Wall

system	number of water in cluster	radii (Å)	height (Å)	area (nm^2)	transform rate	
					ns^{-1}	mol m^{-2} s^{-1}
1.8	3440	33.9	97.2	207.1	1.06	8.50
1.5	2505	30.6	109.8	211.0	1.09	8.58
vesicle[a]	1143	32.8		135.5	0.79	9.68

[a]All vesicle data are obtained from ref 30.

https://doi.org/10.1021/acsomega.2c06381
ACS Omega 2022, 7, 45598−45608

4. CONCLUSIONS

In summary, MD simulation of the self-aggregation behavior of [C_{12}mim][Sal] in aqueous solution was performed, and the entire process of IL aggregation into tubular clusters was obtained. ILs rapidly gathered and formed a funnel-shaped surface in a short time, and then, a process of zipping was observed, forming a complete tubular structure at about 150 ns. The point cloud fitting method was used to obtain the equation of the tubular cluster for the first time, and the tubular cluster structure was analyzed in detail. The anion and imidazolium ring of the cation are distributed on the interface between the tubular cluster and water, while the intermediate part is the alkyl chain of the cation. The inner and outer walls of the tubular cluster are monolayer structures. The radius of the tubular cluster is different in the two systems, but the wall thickness of the two is almost the same. The cationic imidazolium ring and anionic benzene ring tend to be perpendicular to the axis of the cylinder. Similar to vesicles, the interactions for cation−anion and anion−water play a key role in the structural stability of tubular clusters. We also calculated the permeability of water molecules through the wall of the cluster, which is lower than that of the vesicles. Based on this study, our understanding as to the formation, structure, and property of IL tubular clusters in aqueous solution was improved on the molecular level. The application of this tubular structure in molecular penetration and exchange may be more interesting and practical, and we hope that our simulation results will be helpful to this.

■ ASSOCIATED CONTENT

Supporting Information

The Supporting Information is available free of charge at https://pubs.acs.org/doi/10.1021/acsomega.2c06381.

RDF of system 1.8, angle distribution of the alkyl chain and benzene ring in system 1.8, and system 1.8 imidazole ring and benzene ring and axis angle distribution (PDF)

■ AUTHOR INFORMATION

Corresponding Author

Guohui Zhou − *School of Chemistry and Chemical Engineering, Qingdao University, Qingdao, Shandong 266071, China;* orcid.org/0000-0002-1737-0863; Email: zhouguohui@qdu.edu.cn

Author

Kun Jiang − *Qingdao University, Qingdao, Shandong 266071, China;* orcid.org/0000-0002-0436-1212

Complete contact information is available at: https://pubs.acs.org/10.1021/acsomega.2c06381

Notes

The authors declare no competing financial interest.

■ ACKNOWLEDGMENTS

We cordially acknowledge the financial support from the Shandong Province for the Postdoctoral Innovation Projects (202003032). The authors thank the High-Grade Talents Plan of Qingdao University for financial support and all the other friends in this work for their direct and indirect help.

■ REFERENCES

(1) Tang, X.; Lv, S.; Jiang, K.; Zhou, G.; Liu, X. Recent development of ionic liquid-based electrolytes in lithium-ion batteries. *J. Power Sources* **2022**, *542*, 231792.

(2) Wei, C.; Fang, T.; Tang, X.; Wang, P.; Liu, X. Nonnegligible Role of Multifunctional MXenes Hosts for Li-S Batteries: Anchoring and Electrocatalysis. *J. Phys. Chem. C* **2022**, *126*, 17066.

(3) Wei, C.; Jiang, K.; Fang, T.; Liu, X. Insight into the adsorption of Imidazolium-based ionic liquids on graphene by first principles simulation. *J. Mol. Liq.* **2021**, *338*, 116641.

(4) Wei, C.; Jiang, K.; Fang, T.; Liu, X. Effects of anions and alkyl chain length of imidazolium-based ionic liquids at the Au (111) surface on interfacial structure: a first-principles study. *Green Chem. Eng.* **2021**, *2*, 402−411.

(5) Zhang, K.; Zhou, G.; Fang, T.; Jiang, K.; Liu, X. Structural Reorganization of Ionic Liquid Electrolyte by a Rapid Charge/Discharge Circle. *J. Phys. Chem. Lett.* **2021**, *12*, 2273−2278.

(6) Zhang, K.; Zhou, G.; Fang, T.; Tang, X.; Liu, X. Different shapes based on ionic liquid leading to a two-stage discharge process. *J. Mater. Chem. A* **2022**, *10*, 7684−7693.

(7) Li, B.; Wang, C.; Zhang, Y.; Wang, Y. High CO2 absorption capacity of metal-based ionic liquids: A molecular dynamics study. *Green Energy Environ.* **2021**, *6*, 253−260.

(8) Sun, W.; Wang, M.; Zhang, Y.; Ding, W.; Huo, F.; Wei, L.; He, H. Protic vs aprotic ionic liquid for CO2 fixation: A simulation study. *Green Energy Environ.* **2020**, *5*, 183−194.

(9) Fang, T.; Meng, X.; Zhou, G.; Jiang, K.; Liu, X. Nonnegligible role of rigidity/flexibility for efficient CO2 separation in SILMs: A molecular dynamics simulation study. *Int. J. Heat Mass Transfer* **2022**, *183*, 122058.

(10) Fang, T.; Meng, X.; Zhou, G.; Jiang, K.; Liu, X. CO2 separation of membranes consisting of Mxene/ILs with X: A perspective from molecular dynamics simulation. *J. Mol. Liq.* **2022**, *349*, 118099.

(11) Ge, M.; Fang, T.; Zhou, G.; Li, C.; Li, Y.; Liu, X. Insight into the dual effect of water on lignin dissolution in ionic liquids. *Int. J. Biol. Macromol.* **2022**, *205*, 178−184.

(12) Li, C.; Fang, T.; Zhou, G.; Ge, M.; Li, Y.; Liu, X. Mechanism and conformation changes for the whole regeneration process of cellulose in pyridinium-based ionic liquids. *Cellulose* **2022**, *29*, 5479−5492.

(13) Meng, X.; Fang, T.; Zhou, G.; Wang, P.; Liu, X. Molecular Simulation Study on CO2 Separation Performance of GO/Ionic Liquid Membrane. *Int. J. Heat Mass Transfer* **2022**, *197*, 123360.

(14) Wang, Z.; Yan, F.; Bai, L.; Zhang, X.; Liu, X.; Zhang, X. Insight into CO2/CH4 separation performance in ionic liquids/polymer membrane from molecular dynamics simulation. *J. Mol. Liq.* **2022**, *357*, 119119.

(15) Zhao, J.; Zhou, G.; Fang, T.; Ying, S.; Liu, X. Screening ionic liquids for dissolving hemicellulose by COSMO-RS based on the selective model. *RSC Adv.* **2022**, *12*, 16517−16529.

(16) Zhang, J.; Wu, X.; Gan, Z.; Zhu, X.; Jin, Y. Unidirectionally aligned diphenylalanine nanotube/microtube arrays with excellent supercapacitive performance. *Nano Res.* **2014**, *7*, 929−937.

(17) Gaitzsch, J.; Huang, X.; Voit, B. Engineering Functional Polymer Capsules toward Smart Nanoreactors. *Chem. Rev.* **2016**, *116*, 1053−1093.

(18) Shimizu, T.; Ding, W.; Kameta, N. Soft-Matter Nanotubes: A Platform for Diverse Functions and Applications. *Chem. Rev.* **2020**, *120*, 2347−2407.

(19) Lei, L. F.; Pan, F. J.; Lindbråthen, A.; Zhang, X. P.; Hillestad, M.; Nie, Y.; Bai, L.; He, X. Z.; Guiver, M. D. Carbon hollow fiber membranes for a molecular sieve with precise-cutoff ultramicropores for superior hydrogen separation. *Nat. Commun.* **2021**, *12*, 268.

(20) Li, Y.; Wang, Y.; Pesch, G. R.; Baune, M.; Du, F.; Liu, X. Rational Design and Numerical Analysis of a Hybrid Floating cIDE Separator for Continuous Dielectrophoretic Separation of Microparticles at High Throughput. *Micromachines* **2022**, *13*, 582.

(21) Li, Y.; Wang, Y.; Wan, K.; Wu, M.; Guo, L.; Liu, X.; Wei, G. On the design, functions, and biomedical applications of high-throughput

dielectrophoretic micro-/nanoplatforms: a review. *Nanoscale* **2021**, *13*, 4330−4358.
(22) Wan, K.; Wang, Y.; Liu, C.; Wei, C.; Lv, S.; Tang, X.; Fang, T.; Zhao, J.; Wei, G.; Qi, P.; Liu, X. Facile synthesis of hierarchical Ti3C2@FeOOH nanocomposites for antimony contaminated wastewater treatment: Performance, mechanisms, reutilization, and sustainability. *Chem. Eng. J.* **2022**, *450*, 138038.
(23) Wang, Y.; Guo, L.; Qi, P.; Liu, X.; Wei, G. Synthesis of Three-Dimensional Graphene-Based Hybrid Materials for Water Purification: A Review. *Nanomaterials* **2019**, *9*, 1123.
(24) Wang, Y.; Xia, K.; Wang, L.; Wu, M.; Sang, X.; Wan, K.; Zhang, X.; Liu, X.; Wei, G. Peptide-Engineered Fluorescent Nanomaterials: Structure Design, Function Tailoring, and Biomedical Applications. *Small* **2021**, *17*, 2005578.
(25) Qian, J.; Yan, R.; Liu, X.; Li, C.; Zhang, X. Modification to solution-diffusion model for performance prediction of nanofiltration of long-alkyl-chain ionic liquids aqueous solutions based on ion cluster. *Green Energy Environ.* **2020**, *5*, 105−113.
(26) Kuroda, K.; Shimada, Y.; Takahashi, K. Hand-holding and releasing between the anion and cation to change their macroscopic behavior in water. *Green Energy Environ.* **2019**, *4*, 127−130.
(27) Wang, H.; Zhang, L.; Wang, J.; Li, Z.; Zhang, S. The first evidence for unilamellar vesicle formation of ionic liquids in aqueous solutions. *Chem. Commun.* **2013**, *49*, 5222−5224.
(28) Wang, H.; Tan, B.; Wang, J.; Li, Z.; Zhang, S. Anion-based pH responsive ionic liquids: design, synthesis, and reversible self-assembling structural changes in aqueous solution. *Langmuir* **2014**, *30*, 3971−3978.
(29) Wang, Y.-L.; Li, B.; Sarman, S.; Mocci, F.; Lu, Z.-Y.; Yuan, J.; Laaksonen, A.; Fayer, M. D. Microstructural and Dynamical Heterogeneities in Ionic Liquids. *Chem. Rev.* **2020**, *120*, 5798−5877.
(30) Jiang, K.; Liu, X.; He, H.; Wang, J.; Zhang, S. Insight into the formation and permeability of ionic liquid unilamellar vesicles by molecular dynamics simulation. *Soft Matter* **2020**, *16*, 2605−2610.
(31) Jiang, K.; Zhou, G.; Fang, T.; Liu, X. Permeability of Vesicles for Imidazolium-Based Ionic Liquids in Aqueous Solution: A Molecular Dynamic Simulation Study. *Ind. Eng. Chem. Res.* **2021**, *60*, 3174−3183.
(32) Tian, T.; Qin, J.; Gao, Y. a.; Yu, L. Experimental and DFT studies on aggregation behavior of dodecylsulfonate-based surface active ionic liquids in water and ethylammonium nitrate. *J. Mol. Liq.* **2016**, *218*, 457−464.
(33) Zhou, L.; Tian, T.; Xiao, J.; Wang, T.; Yu, L. Aggregation behavior of pyrrolidinium-based surface active ionic liquids in H 2 O-EAN binary solvents. *J. Mol. Liq.* **2017**, *225*, 50−55.
(34) Lépori, C. M. O.; Correa, N. M.; Silber, J. J.; Falcone, R. D.; López-López, M.; Moyá, M. L. Use of Ionic Liquids-like Surfactants for the Generation of Unilamellar Vesicles with Potential Applications in Biomedicine. *Langmuir* **2019**, *35*, 13332−13339.
(35) Li, Z.; Shi, Y.; Zhu, A.; Zhao, Y.; Wang, H.; Binks, B. P.; Wang, J. Light-Responsive, Reversible Emulsification and Demulsification of Oil-in-Water Pickering Emulsions for Catalysis. *Angew. Chem., Int. Ed.* **2021**, *60*, 3928−3933.
(36) Kandasamy, S.; Moniruzzaman, M.; Sivapragasam, M.; Shamsuddin, M. R.; Mutalib, M. I. A. Formulation and characterization of acetate based ionic liquid in oil microemulsion as a carrier for acyclovir and methotrexate. *Sep. Purif. Technol.* **2018**, *196*, 149−156.
(37) Pyne, A.; Kundu, S.; Banerjee, P.; Sarkar, N. Unveiling the Aggregation Behavior of Doxorubicin Hydrochloride in Aqueous Solution of 1-Octyl-3-methylimidazolium Chloride and the Effect of Bile Salt on These Aggregates: A Microscopic Study. *Langmuir* **2018**, *34*, 3296−3306.
(38) Kong, J.; He, H. Challenge and opportunity of ionic liquids-An interview with Prof. Douglas R. Macfarlane. *Green Energy Environ.* **2020**, *5*, 243−245.
(39) Zhou, G.; Jiang, K.; Zhang, Y.; Wang, Z.; Liu, X. Insight into the properties and structures of vapor-liquid interface for imidazolium-based ionic liquids by molecular dynamics simulations. *J. Mol. Liq.* **2021**, *326*, 115295.
(40) Liu, X.; Yao, X.; Wang, Y.; Zhang, S. Mesoscale structures and mechanisms in ionic liquids. *Particuology* **2020**, *48*, 55−64.
(41) Zhou, G.; Jiang, K.; Wang, Z.; Liu, X. Insight into the behavior at the hygroscopicity and interface of the hydrophobic imidazolium-based ionic liquids. *Chin. J. Chem. Eng.* **2021**, *31*, 42−55.
(42) Luo, H.; Jiang, K.; Liang, X.; Liu, H.; Li, Y. Small molecule-mediated self-assembly behaviors of Pluronic block copolymers in aqueous solution: impact of hydrogen bonding on the morphological transition of Pluronic micelles. *Soft Matter* **2020**, *16*, 142−151.
(43) Guo, C.; Luo, Y.; Zhou, R.; Wei, G. Probing the self-assembly mechanism of diphenylalanine-based peptide nanovesicles and nanotubes. *ACS Nano* **2012**, *6*, 3907−3918.
(44) Niemann, T.; Zaitsau, D.; Strate, A.; Villinger, A.; Ludwig, R. Cationic clustering influences the phase behaviour of ionic liquids. *Sci. Rep.* **2018**, *8*, 14753−14760.
(45) Khudozhitkov, A. E.; Neumann, J.; Niemann, T.; Zaitsau, D.; Stange, P.; Paschek, D.; Stepanov, A. G.; Kolokolov, D. I.; Ludwig, R. Hydrogen Bonding Between Ions of Like Charge in Ionic Liquids Characterized by NMR Deuteron Quadrupole Coupling Constants-Comparison with Salt Bridges and Molecular Systems. *Angew. Chem., Int. Ed.* **2019**, *58*, 17863−17871.
(46) Sharma, A.; Bhargava, B. L. Self-Assembly of Cations in Aqueous Solutions of Multiheaded Cationic Surfactants: All Atom Molecular Dynamics Simulation Studies. *J. Phys. Chem. B* **2018**, *122*, 10943−10952.
(47) Nadimi, H.; Housaindokht, M. R.; Moosavi, F. The effect of anion on aggregation of amino acid ionic liquid: Atomistic simulation. *J. Mol. Graphics Modell.* **2020**, *101*, 107733.
(48) Zhou, J.; Liu, X. M.; Zhang, S. J.; Zhang, X. P.; Yu, G. R. Effect of small amount of water on the dynamics properties and microstructures of ionic liquids. *AlChE J.* **2017**, *63*, 2248−2256.
(49) Liu, X. M.; Zhou, G. H.; Huo, F.; Wang, J. J.; Zhang, S. J. Unilamellar Vesicle Formation and Microscopic Structure of Ionic Liquids in Aqueous Solutions. *J. Phys. Chem. C* **2016**, *120*, 659−667.
(50) Schmid, N.; Eichenberger, A. P.; Choutko, A.; Riniker, S.; Winger, M.; Mark, A. E.; van Gunsteren, W. F. Definition and testing of the GROMOS force-field versions 54A7 and 54B7. *Eur. Biophys. J. Biophys.* **2011**, *40*, 843−856.
(51) Malde, A. K.; Zuo, L.; Breeze, M.; Stroet, M.; Poger, D.; Nair, P. C.; Oostenbrink, C.; Mark, A. E. An Automated Force Field Topology Builder (ATB) and Repository: Version 1.0. *J. Chem. Theory Comput.* **2011**, *7*, 4026−4037.
(52) Toukan, K.; Rahman, A. Molecular-dynamics study of atomic motions in water. *Phys. Rev. B: Condens. Matter* **1985**, *31*, 2643−2648.
(53) Martínez, L.; Andrade, R.; Birgin, E. G.; Martínez, J. M. PACKMOL: A Package for Building Initial Configurations for Molecular Dynamics Simulations. *J. Comput. Chem.* **2009**, *30*, 2157−2164.
(54) Van Der Spoel, D.; Lindahl, E.; Hess, B.; Groenhof, G.; Mark, A. E.; Berendsen, H. J. GROMACS: fast, flexible, and free. *J. Comput. Chem.* **2005**, *26*, 1701−1718.
(55) Abraham, M. J.; Murtola, T.; Schulz, R.; Páll, S.; Smith, J. C.; Hess, B.; Lindahl, E. GROMACS: High performance molecular simulations through multi-level parallelism from laptops to supercomputers. *SoftwareX* **2015**, *1−2*, 19−25.
(56) Darden, T.; York, D.; Pedersen, L. Particle Mesh Ewald—an N.Log(N) Method for Ewald Sums in Large Systems. *J. Chem. Phys.* **1993**, *98*, 10089−10092.
(57) Yan, Y.; Wang, J. Cylindrical fitting method of laser scanner point cloud data. *Sci. Surv. Mapp.* **2018**, *43*, 83−87.
(58) Humphrey, W.; Dalke, A.; Schulten, K. VMD: Visual molecular dynamics. *J. Mol. Graphics Modell.* **1996**, *14*, 33−38.
(59) Xu, W.; Wang, T.; Cheng, N.; Hu, Q.; Bi, Y.; Gong, Y.; Yu, L. Experimental and DFT studies on the aggregation behavior of imidazolium-based surface-active ionic liquids with aromatic counterions in aqueous solution. *Langmuir* **2015**, *31*, 1272−1282.

https://doi.org/10.1021/acsomega.2c06381
ACS Omega 2022, 7, 45598−45608